

Dimensional Reduction and Odd-Frequency Pairing of the Checkerboard-Lattice Hubbard Model at 1/4-Filling

Yuki Yanagi^{1*}, Yasufumi Yamashita^{2†} and Kazuo Ueda¹

¹ Institute for Solid State Physics, University of Tokyo, Kashiwa, Chiba 277-8581, Japan

² College of Engineering, Nihon University, Koriyama, Fukushima 963-8642, Japan

The ferromagnetism of the checkerboard-lattice Hubbard model at quarter filling is one of the few exact ferromagnetic ground states known in the family of Hubbard models. When the nearest neighbor hopping, t_1 , is negligible compared with the second neighbor one, t_2 , the system reduces to a collection of Hubbard chains. We find that the 1D character is surprisingly robust as long as $t_1 < t_2$. This phenomenon of dimensional reduction due to the geometrical frustration leads to peculiar magnetic orders with 1D character for intermediate U and is responsible for odd-frequency superconducting states close to the magnetic boundary.

KEYWORDS: checkerboard-lattice Hubbard model, flat-band, ferromagnetism, dimensional reduction, odd-frequency superconductivity

Strongly correlated electron systems (SCES) with geometrical frustration show a variety of fascinating physics.¹⁻⁸⁾ The Hubbard model on the two-dimensional pyrochlore lattice, called checkerboard-lattice (CB-lattice) Hubbard model, is one typical example and its intriguing properties, such as the metal-insulator transition at 1/2-filling^{5,8)} and the ferromagnetism at 1/4-filling^{1,2)} have been studied by many authors. The latter is known as the flat-band ferromagnetism. Mielke have rigorously proved that the complete ferromagnetic state is the ground state of the CB-lattice Hubbard model at 1/4-filling at the symmetric point $t_1 = t_2$,¹⁾ where t_1 and t_2 are the nearest and next nearest neighbor hoppings, respectively [see Fig. 1 (a)]. According to the numerical calculation, this ferromagnetic state is extended to the case that $t_1 > t_2$.²⁾ The electronic states including the ferromagnetism for $t_1 < t_2$, however, have not been investigated so far.

In the SCES, the electrons move trying to avoid each other in space and time due to the strong local Coulomb repulsion and it is difficult for them to condense into the isotropic pairing state where the on-site and equal-time gap function $\Delta(\mathbf{r} = \mathbf{0}, t = 0)$ is finite with \mathbf{r} and t being the relative coordinate and time of the Cooper pairs. One possible way to stabilize superconductivity in SCES is to form spatially anisotropic Cooper pairs, i.e. $\Delta(\mathbf{r} = \mathbf{0}, t) = 0$ and such pairing states are considered to be realized in most of the SCES.⁹⁾ An alternative way is to make the equal-time gap function $\Delta(\mathbf{r}, t = 0)$ vanish. In other words, the gap function has odd-frequency dependence $\Delta(\mathbf{r}, \omega) = -\Delta(\mathbf{r}, -\omega)$. The odd-frequency pairing state was first proposed by Berezinskii in the context of the ³He.¹⁰⁾ After his proposal, theoretical studies on the odd-frequency pairing have been performed by several authors¹¹⁻¹⁸⁾ and several models have been proposed as playgrounds for realization of the odd-frequency pairing. Based on these studies, it has been pointed out that there are several favorable conditions for the odd-frequency pairing: (1) strong retardation effects, (2) geometrical frustration and (3) one-dimensionality. (1) When the retardation effects are strong, the effective interaction for the odd-frequency pairing is at-

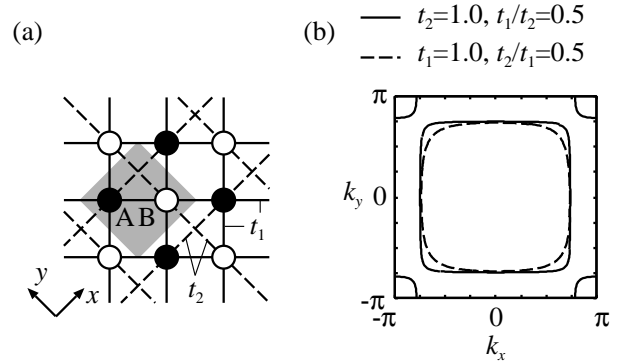


Fig. 1. (Color online) (a) Schematic of the CB-lattice. The solid and dashed lines represent t_1 and t_2 hoppings, respectively. The shaded region is the unit cell including two distinct sites A and B denoted by the filled and open circles. (b) Fermi surfaces for $t_2 = 1.0$ and $t_1/t_2 = 0.5$ (solid lines) and for $t_1 = 1.0$ and $t_2/t_1 = 0.5$ (dashed lines).

tractive for a wide range in frequency space and can dominate over the one for the even-frequency pairing.¹⁸⁾ Strong retardation is realized in a SCES near a quantum critical point (QCP)¹⁵⁾ and also in an electron-phonon system with anomalously soft phonons.¹⁸⁾ (2) It has been shown that a geometrical frustration tends to suppress even-frequency spin-singlet pairing correlation and as a result, enhance the odd-frequency pairing correlation.^{14,17)} (3) In the quasi-one-dimensional system, it has been shown that the odd-frequency spin-singlet p -wave pairing is favored when the one-dimensionality is strong.¹⁷⁾ In this case, the nodes of the gap function for the p -wave pairing do not intersect the Fermi surfaces and the pairing interaction is effective in a wide region of the momentum space. Although it is obvious that the conditions (1) and (2) are satisfied in the CB-lattice Hubbard model near the QCP, we will show that the condition (3) is also satisfied in the model.

In this letter, we investigate magnetic properties and superconductivity of the CB-lattice Hubbard model at 1/4-filling by using the mean field approximation, exact diagonalization (ED) method and random phase approximation (RPA). We

*E-mail address: yanagi@issp.u-tokyo.ac.jp

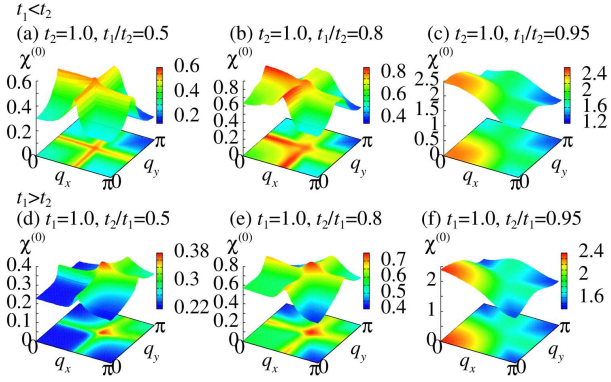


Fig. 2. (Color online) (a)-(c) q -dependence of the largest eigenvalue of the bare susceptibility $\chi_{1st}^{(0)}(\mathbf{q})$ for $t_1 < t_2$ at $T = 0.02t_2$ and (d)-(f) that for $t_1 > t_2$ at $T = 0.02t_1$.

show that the charge and magnetic ordered states with one-dimensional character are observed in the CB-lattice Hubbard model for $t_1 < t_2$. The spin fluctuations also have strong 1D structure and promote the odd-frequency spin-singlet p -wave superconductivity.

This remarkable property of the quasi-one-dimensionality is a consequence of the geometrical frustration of the present model, which may be characterized by dimensional reduction. We will show that the odd-frequency spin-singlet p -wave state is stabilized in an extremely wide parameter range in this model.

Let us first examine single-electron properties of the CB-lattice Hubbard model at $1/4$ filling. When $t_1/t_2 = 0$, there are two 1D bands along k_x and k_y directions, each to be labeled by A- and B-band. Fermi surfaces for the A- and B-bands are respectively located along $k_x = \pm 3\pi/4$ and $k_y = \pm 3\pi/4$, since both t_1 and t_2 are positive definite in this paper. Looking at the largest eigenvalue of the non-interacting paramagnetic susceptibility (denoted by $\chi_{1st}^{(0)}(\mathbf{q})$ hereafter), the perfect nesting vectors of $\mathbf{q} = (\pi/2, q_y)$ and $(q_x, \pi/2)$ give ridge-like structures, which are hallmarks of the one dimensionality. With increasing t_1 from zero toward t_2 , the A- and B-bands start to hybridize and we expect that the 1D band structures would be modified significantly. Strikingly enough, though, the shape of Fermi surface does not change much, except for the small regions centered around the Fermi-surface crossing points at $(k_x, k_y) = (\pm 3\pi/4, \pm 3\pi/4)$ [see Fig. 1(b)]. As a result, a major Fermi surface of a large hole pocket around Γ point looks square-like and retains one dimensionality even for $t_1/t_2 = 0.8$. This is because the 1D-like Fermi surface at $1/4$ filling lies in the vicinity of the zone boundary of the first Brillouin zone where A-B band mixings vanish exactly from the symmetry.¹⁹⁾ The 1D nature of Fermi surface is also seen in $\chi_{1st}^{(0)}(\mathbf{q})$ as ridge-like structures along $q_x = \pi/2$ and $q_y = \pi/2$ lines as shown in Figs. 2-(a) and (b). Along the ridge line, there is a weak structure and the most divergent mode is located at $\mathbf{q} = (\pi/2, \pi/2)$ for $0 < t_1/t_2 < 0.58$ and at about $\mathbf{q} = (\pi/2, 0)$ and $(0, \pi/2)$ for $0.66 < t_1/t_2 < 0.91$. In many cases, the geometrical frustration suppresses the q -dependence of the spin fluctuations, leading to suppression of the even-frequency anisotropic pairing.^{14,17)} On the other hand, in the CB-lattice, it produces the above-mentioned ro-

bust 1D features of the single-electron properties and promotes the odd-frequency pairing as explained later.

On the other hand for $0 < t_2/t_1 < 0.9$, the Fermi surface is a single rounded-square electron pocket [Fig. 1(b)] and $\chi_{1st}^{(0)}(\mathbf{q})$ has an incommensurate peak located at $\mathbf{q} = (\pi/2 + \delta, \pi/2 + \delta)$ with $\delta \sim 0.1$. Note that the ridge-like structures around $q_x = \pi/2$ and $q_y = \pi/2$ develop with increasing t_2/t_1 , see Figs. 2(d) and (e). As we approach the Mielke point by changing t_2/t_1 or t_1/t_2 to unity, due to the geometrically frustrated hopping processes, the lower band is flattened and $\chi_{1st}^{(0)}(\mathbf{q})$ become nearly-structureless with a weak peak located at $\mathbf{q} = (0, 0)$ for $t_1/t_2 \sim 1$ as shown in Figs. 2(c) and (f). Near the Mielke point, therefore, strong electron correlation is intrinsic even when U is rather small compared with t_1 and t_2 .

After switching on the Coulomb interaction U , within the mean-field approximation, the peak modes in $\chi_{1st}^{(0)}(\mathbf{q})$ become leading magnetic instabilities from the paramagnetic phase and second-order phase transition takes place at a certain value of U_c for a fixed t_1/t_2 . When $t_1/t_2 = 1$, we know that the Mielke's ferromagnetism is realized irrespective of U , meaning that $U_c(t_1/t_2 = 1) = 0$. Exact diagonalization (ED) study for 16-site CB-lattice Hubbard model under anti-periodic boundary conditions shows that a critical U_c from the paramagnetic ($S = 0$) to the ferromagnetic ($S = 4$) states grows rapidly by changing t_1/t_2 or t_2/t_1 from unity, like $U_c(t_2/t_1 = 0.8) = 4.0537t_1$ or $U_c(t_1/t_2 = 0.8) = 4.5105t_2$.^{2,19)} Since the flat-band ferromagnetism would be suppressed when the bands become dispersive, we consider the magnetic phase diagram in U - t_1 or U - t_2 plane by applying the mean-field approximation. For this purpose, a unit cell is extended to the $2\sqrt{2} \times 2\sqrt{2}$ ones shown in the inset of Fig. 3 and set up charge-modulated antiferromagnets (AFs) of line-, plaquette-, and checkerboard-type as well as usual paramagnet (PM) and ferromagnet (FM), for possible mean-field ground states. The line- and plaquette-AF have $\mathbf{q} = (\pi/2, \pi/2)$ spin structure and are made from different arrangements of classical charge and spin ordered chains along the t_2 -bond directions at $1/4$ -filling. In the case of $t_2/t_1 < 1$ and relatively large U , the checkerboard-type AF ground state is expected, since the charge modulation in this state are so distributed as to gain kinetic energy through t_1 hoppings. These states are consistent with the short-range correlations calculated by ED. Fig. 3 shows the magnetic mean-field phase diagram in U - t_1 (left panel) or U - t_2 plane (right) as well as the RPA instabilities. The self-consistent energy of the different ordered states are typically calculated for a 32×32 number of enlarged unit cells at $T = 0.01t_1$ for $t_2/t_1 < 1$ or at $T = 0.01t_2$ for $t_1/t_2 < 1$.¹⁹⁾ From Fig. 3, one can see that Mielke's ferromagnetic phase is extended for large- U region and various AF phases emerge between the paramagnetic and ferromagnetic phases. When $0 < t_1/t_2 < 0.2$, the self-consistent energy of the line- and the plaquette-states are almost degenerate owing to the one-dimensionality of the system, which may lead to the discrepancy between the phase boundary estimated by the mean-field calculation at $T = 0.01t_2$ and that by RPA at $T = 0.02t_2$. It should be also mentioned that, because of the size limitation of the unit cell in the mean-field approximation, we could not reproduce the second-order phase boundary from PM to the incommensurate state found in $\chi_{1st}^{(0)}$ for $t_1 > t_2$. It is natural to expect that there would be successive phase transitions be-

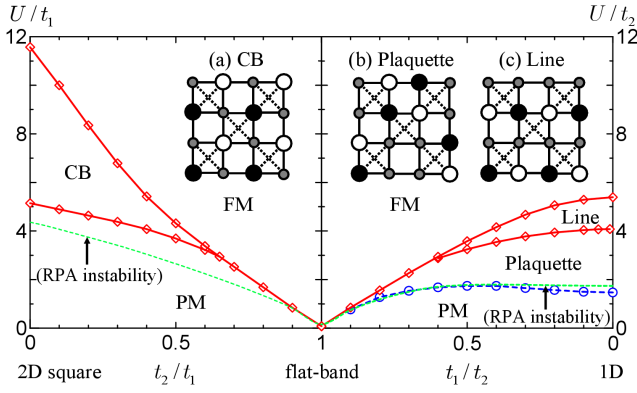


Fig. 3. (Color online) Mean-field phase diagram for $t_2 < t_1$ (left-half panel) and $t_2 > t_1$ (right). The open circles and diamonds are, respectively, continuous and discontinuous phase-transition points within the present numerical accuracy. RPA-instability lines are also depicted by the dotted lines. Inset figures (a)-(c) show the unit cells of various charge-ordered AF state, where the circular radius stands for the magnitude of charge density and each color zero (gray), positive (black), or negative (white) spin polarization.

shown in Fig. 3.

Now, let us turn our attention to the superconductivity. We investigate the superconductivity by solving the following linearized Eliashberg equation within the RPA,

$$\lambda \Delta_{\alpha\beta}(k) = -\frac{T}{N} \sum_{k'} \sum_{\alpha'\beta'} V_{\alpha\beta}(k-k') \times G_{\alpha'\alpha}^{(0)}(-k') \Delta_{\alpha'\beta'}(k') G_{\beta'\beta}^{(0)}(k'), \quad (1)$$

where $G_{\alpha\beta}^{(0)}(k)$ is the noninteracting Green's function, $\Delta_{\alpha\beta}(k)$ is the gap function, $V_{\alpha\beta}(q)$ is the effective pairing interaction and λ is the eigenvalue of the eigenvalue equation (1) which represents the strength of the superconducting correlation and reaches unity at $T = T_c$. In the RPA, $V_{\alpha\beta}(q)$ is given as,

$$\hat{V}(q) = \eta U^2 \hat{\chi}^s(q) - \frac{1}{2} U^2 \hat{\chi}^c(q) + U, \quad (2)$$

where $\eta = 3/2(-1/2)$ for the spin-singlet (-triplet) state and the spin (charge) susceptibility $\hat{\chi}^{s(c)}(q)$ is given as, $\hat{\chi}^{s(c)}(q) = [\hat{1} - (+)U \hat{\chi}^{(0)}(q)]^{-1} \hat{\chi}^{(0)}(q)$ with the bare susceptibility $\chi_{\alpha\beta}^{(0)}(q) = -T/N \sum_k G_{\alpha\beta}^{(0)}(k) G_{\beta\alpha}^{(0)}(k-q)$. We use the abbreviations $k = (\mathbf{k}, i\varepsilon_n)$ and $q = (\mathbf{q}, i\omega_m)$, where $\varepsilon_n = (2n+1)\pi T$ and $\omega_m = 2m\pi T$. In the numerical calculations, we use the 128×128 k -meshes in the 1st Brillouin zone and 512 Matsubara frequencies ($-511\pi T \leq \varepsilon_n \leq 511\pi T$) and set $T = 0.02t_1$ and $T = 0.02t_2$ for $t_1 > t_2$ and $t_1 < t_2$, respectively.

Fig 4 shows the k - and the ε_n -dependence of the obtained gap functions for several typical parameter sets in the cases that $t_1 < t_2$, $t_1 > t_2$ and $t_1 \sim t_2$, where the values of U are chosen as the largest eigenvalue $\lambda \sim 1$. We note that in the present case, the effective pairing interaction given in eq. (2) can be approximated by $\hat{V}(q) \sim \eta U^2 \hat{\chi}^s(q)$, that is, the superconductivity is driven by the spin fluctuations because the spin fluctuations always dominate over the charge fluctuations and are strongly enhanced by the Coulomb interaction U when $\lambda \sim 1$. With these in mind, we discuss the pairing symmetry and mechanism. It is found that the pairing symmetry for $t_1 = 1.0$ and $t_2/t_1 = 0.5$ is even-frequency spin-singlet s -wave (ES) pairing as shown in Fig. 4 (a) and (d). Since the

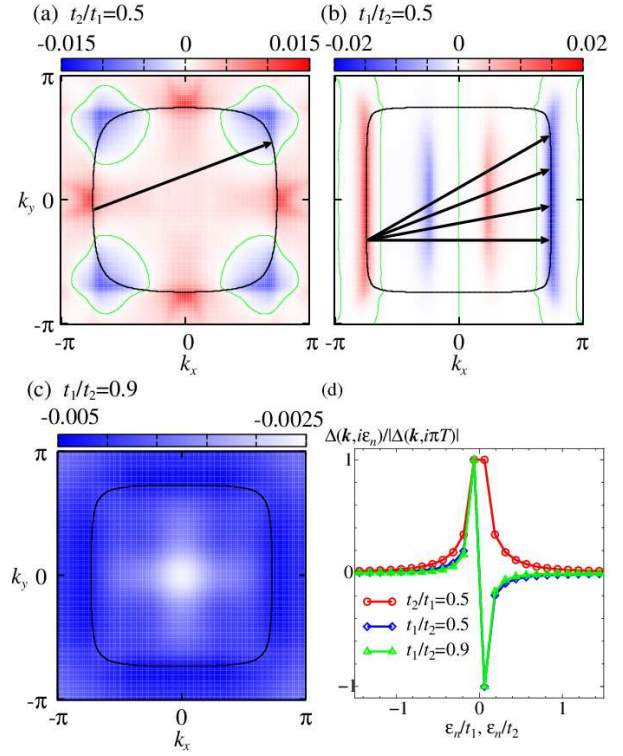


Fig. 4. (Color online) (a), (b) and (c) k -dependence of the lower band diagonal component of the gap function $\Delta(\mathbf{k}, i\varepsilon_n)$ with the lowest Matsubara frequency $\varepsilon_n = \pi T$ for $t_1 = 1.0$ and $t_2/t_1 = 0.5$, $t_2 = 1.0$ and $t_1/t_2 = 0.5$ and $t_2 = 1.0$ and $t_1/t_2 = 0.9$, respectively. The black and green (gray) lines denote the Fermi surfaces and the nodes of the gap function, respectively and the arrows schematically represent the typical pair scatterings. (d) ε_n -dependence of that on the Fermi surface $\mathbf{k} = \mathbf{k}_F \sim (3\pi/4, 0)$

effective pairing interaction for the spin-singlet state given in eq. (2) has a sharp peak at $\mathbf{q} \sim (\pi/2, \pi/2)$ reflecting the structure of $\hat{\chi}^{(0)}(q)$ shown in Fig. 2 (d), strong repulsive pair scatterings with momentum transfer $\mathbf{q} \sim (\pi/2, \pi/2)$ take place [see Fig. 4 (a)]. Then, the gap function has different signs at the segments on the Fermi surface which are connected to each other by $\mathbf{q} \sim (\pi/2, \pi/2)$.

On the other hand, the pairing symmetry for $t_2 = 1.0$ and $t_1/t_2 = 0.5$ is odd-frequency spin-singlet p -wave (OSP) as shown in Figs. 4 (b) and (d). Since the effective pairing interaction for the spin-singlet state given in eq. (2) has ridge-like structures along $q_x = \pi/2$ and $q_y = \pi/2$, strong repulsive pair scatterings with momentum transfer $\mathbf{q} \sim (\pi/2, q_y)$ and $\mathbf{q} \sim (q_x, \pi/2)$ are important. Therefore, electrons on the Fermi surface with $k_x \sim -3\pi/4$ ($k_y \sim -3\pi/4$) are scattered to the other section of the Fermi surface with $k_x \sim 3\pi/4$ ($k_y \sim -3\pi/4$) and vice versa [see Fig. 4 (b)]. Then, the gap function has sign change between the sections of the Fermi surface which are connected to each other by $\mathbf{q} \sim (\pi/2, q_y)$ and the resulting k -dependence of the gap function is p_x -wave. We note that the p_x - and p_y -wave states are degenerate in the CB-lattice. Since the relation $\Delta(\mathbf{k}, i\varepsilon_n) = \Delta(-\mathbf{k}, -i\varepsilon_n)$ has to be hold for the spin-singlet state, the frequency-dependence of the gap function is odd.

In contrast to the above-mentioned two cases, near the Mielke point, the spin-triplet and spatially isotropic state, i.e., the odd-frequency spin-triplet s -wave (OTS) pairing is realized as shown in Fig. 4 (c) and (d). Near the Mielke

point, the lower bandwidth is narrow and the q -dependence of $\hat{\chi}^{(0)}(q)$ is weak as shown in Figs. 2 (c) and (f). Then, the q -dependence of the effective pairing interaction for the spin-triplet state given in eq. (2) is also weak and $V(q) < 0$ for any q which lead to strong attractive pair scatterings. Thus, the gap function shows no sign change and is of s -wave. Since $\Delta(\mathbf{k}, i\varepsilon_n) = -\Delta(-\mathbf{k}, -i\varepsilon_n)$ has to hold for the spin-triplet state, the frequency-dependence of the gap function is odd. Two distinct odd-frequency pairing states, the OSp and OTs states are realized due to the spin fluctuations with quite different features characterized by the strong one-dimensionality on one hand and by the weak q -dependence on the other hand.

Finally, we show the superconducting phase diagram in the t_1 - and t_2 - U planes in Fig. 5, where the superconducting phase boundary are defined as the points at which the largest eigenvalue of eq. (1) λ reaches unity. For $t_1 > t_2$, the ESs pairing is realized in the wide range of t_2/t_1 near the magnetic ordered phase with the ordering vector $\mathbf{q} \sim (\pi/2, \pi/2)$ [see Figs. 2 (d) and (e) and Fig. 3]. On the other hand, for $t_1 < t_2$, the OSp state is realized in the extremely wide range of t_1/t_2 . This situation is in a striking contrast to the usual quasi-one-dimensional Hubbard model, where the one-dimensionality is lost rapidly with increasing inter-chain hoppings leading to suppression of the OSp pairing correlation. The OSp pairing is realized also for $t_1 > t_2$ ($0.73 \leq t_2/t_1 \leq 0.83$) because there the 1D structure of $\hat{\chi}^{(0)}(q)$ develops as shown in Fig. 2 (e). Remarkably, the OSp pairing emerges already for moderate enhancement of the spin fluctuations, whereas the ESs pairing necessitates the very strong enhancement, which indicates the robustness of the OSp pairing.¹⁷⁾ It is worthwhile to note that for $t_1 < t_2$, the ESs state is second dominant in the wide range of t_1/t_2 . The gap function for this ESs pairing, however, have no nodes on the Fermi surfaces in contrast to the case that $t_1 > t_2$ because the Fermi surfaces are disconnected.²⁰⁾ It is similar to the s_{\pm} -wave state discussed for the iron-based superconductors.²¹⁻²³⁾ At 1/4-filling, the Fermi surface around $\mathbf{k} = (\pi, \pi)$ is smaller than that around $\mathbf{k} = (0, 0)$ and the resulting T_c for the ESs state is relatively low, while near 1/2-filling, the Fermi surfaces around $\mathbf{k} = (\pi, \pi)$ is comparable in size as that around $\mathbf{k} = (0, 0)$, and the resulting T_c is relatively high (not shown).¹⁹⁾ Near the Mielke point, the OTs state is realized due to the spin fluctuations with featureless q -dependence. It should be pointed out that when the q -dependence of the spin fluctuations are weak, the mode-mode coupling effects of the various fluctuations are considered to become important. Thus, the vertex corrections as well as the self-energy corrections³⁾ neglected in the RPA may play significant roles for the stability of the OTs pairing near the Mielke point. We note that with decreasing temperature, the OTs region shrinks and the ESs region for $t_1 > t_2$ and the OSp region for $t_1 < t_2$ are extended toward the Mielke point because the q -dependence of the spin fluctuations gets stronger. Therefore, further investigations beyond the RPA study are needed to clarify whether the OTs pairing near the Mielke point eventually survives at lower temperatures.

Here, we briefly comment on the re-entrant feature of the odd-frequency pairing previously reported.^{15,18)} In the present study, we have not observed any clear re-entrant feature down to $T = 0.01t_1$ or $T = 0.01t_2$.

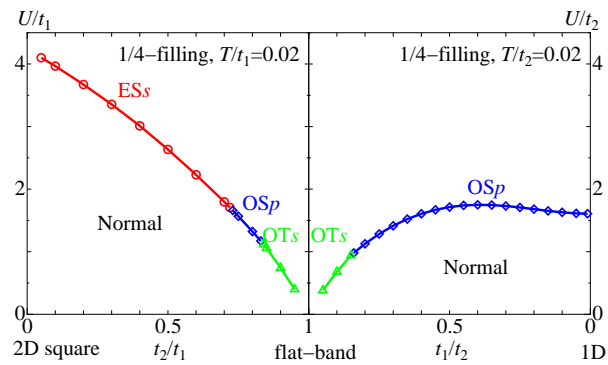


Fig. 5. (Color online) Phase diagram on the t_1 - and t_2 - U planes, where the open circles, diamonds and triangles denote the ESs , OSp and OTs pairing instabilities, respectively.

and the superconductivity in the CB-lattice Hubbard model at 1/4-filling with use of the mean field approximation, ED method and RPA. We have shown that the model exhibits the one-dimensional charge and magnetic orders, such as the plaquette and line orders. The spin fluctuations have also the one-dimensional feature, i.e., the ridge-like structures in the momentum space and drives the OSp superconductivity in the extremely wide range of t_1/t_2 . These phenomena are due to the 1D nature of the CB-lattice Hubbard model which is quite robust against the inter-chain hopping t_1 in contrast to the case of the usual quasi-1D Hubbard model.

Acknowledgment This work has been supported by a Grant-in-Aid for Scientific Research on Innovative Areas “Heavy Electrons” (No. 20102008) of The Ministry of Education, Culture, Sports, Science, and Technology, Japan.

- 1) A. Mielke: J. Phys. A: Math. Gen. **24** (1991) L73; **24** (1991) 3311.
- 2) K. Kusakabe and H. Aoki: Physica B **194-196** (1994) 215.
- 3) M. Isoda and S. Mori: J. Phys. Soc. Jpn. **69** (2000) 1509.
- 4) H. Tsunetsugu: J. Phys. Soc. Jpn. **71** (2002) 1844.
- 5) S. Fujimoto: Phys. Rev. Lett. **89** (2002) 226402.
- 6) Y. Yamashita and K. Ueda: Phys. Rev. B **67** (2003) 195107.
- 7) R. Arita, K. Held, A. V. Lukoyanov and V. I. Anisimov: Phys. Rev. Lett. **98** (2007) 166402.
- 8) T. Yoshioka, A. Koga and N. Kawakami: J. Phys. Soc. Jpn. **77** (2008) 104702.
- 9) M. Sgrist and K. Ueda: Rev. Mod. Phys. **63** (1991) 239.
- 10) V. L. Berezinskii: JETP Lett. **20** (1974) 287.
- 11) A. V. Balatsky and E. Abrahams: Phys. Rev. B **45** (1992) 13125.
- 12) P. Coleman, E. Miranda and A. Tsvelik: Phys. Rev. Lett. **70** (1993) 2960.
- 13) N. Bulut, D. J. Scalapino and S. R. White: Phys. Rev. B **47** (1993) 14599.
- 14) M. Vojta and E. Dagotto: Phys. Rev. B **59**(1999) R713.
- 15) Y. Fuseya, H. Kohno and K. Miyake: J. Phys. Soc. Jpn. **72** (2003) 2914.
- 16) T. Hotta: J. Phys. Soc. Jpn. **78** (2009) 123710.
- 17) K. Shigeta, S. Onari, K. Yada and Y. Tanaka: Phys. Rev. B **79** (2009) 174507.
- 18) H. Kusunose, Y. Fuseya and K. Miyake: J. Phys. Soc. Jpn. **80** (2011) 044711.
- 19) Y. Yamashita, Y. Yanagi, and K. Ueda: private communication.
- 20) K. Kuroki and R. Arita: Phys. Rev. B **64** (2001) 024501.
- 21) I. I. Mazin, D. J. Singh, M. D. Johannes, and M. H. Du: Phys. Rev. Lett. **101** (2008) 057003.
- 22) Kuroki, S. Onari, R. Arita, H. Usui, Y. Tanaka, H. Kontani, and H. Aoki: Phys. Rev. Lett. **101** (2008) 087004.
- 23) Y. Yanagi, Y. Yamakawa and Y. Ōno: Phys. Rev. B **81** (2010) 054518.